# Finite Larmor radius effects on test particle transport in drift wave-zonal flow turbulence

**J.M. Dewhurst[1], B. Hnat[1] and R.O. Dendy[2,1]**

[1] Centre for Fusion, Space and Astrophysics, Department of Physics, Warwick University, Coventry CV4 7AL, U.K.
[2] Euratom/UKAEA Fusion Association, Culham Science Centre, Abingdon, Oxfordshire OX14 3DB, U.K.

E-mail: `j.m.dewhurst@warwick.ac.uk`

**Abstract.** The effect of finite Larmor radius on the transport of passive charged test particles moving in turbulent electrostatic fields is investigated. The turbulent field is governed by a flexible model which is able to produce turbulence where zonal flows are damped or free to self-generate. A subtle interplay between trapping in small scale vortices and entrainment in larger scale zonal flows determines the rate, character and Larmor radius dependence of the test particle transport. When zonal flows are damped, the transport is classically diffusive, with Gaussian statistics, and the rate of transport decreases with increasing Larmor radius. Once the Larmor radius is larger than the typical radius of the turbulent vortices, the rate of transport remains roughly constant. When zonal flows are allowed non-Gaussian statistics are observed. Radial transport (across the zones) is subdiffusive and decreases with the Larmor radius at a slower rate. Poloidal transport (along the zones), however, is superdiffusive and increases with small values of the Larmor radius.

## 1. Introduction

The majority of cross-field particle and energy transport in magnetically confined plasma can be attributed to low frequency turbulent fluctuations. The drift instability provides a mechanism for the generation of such fluctuations in the presence of a background density gradient perpendicular to the magnetic field. The edge region of magnetically confined plasmas, with increased collisionality and large density gradients, offers ideal conditions for the drift instability to occur. The nonlinear nature of turbulent dynamics distributes energy extracted from the background density gradient into modes with different wave numbers. It has been observed that some of the energy is deposited into small wave number modes, generating large flows which in tokamaks manifest as poloidally extended and radially localised coherent structures. These modes, with finite radial wave numbers but vanishing poloidal and toroidal numbers ($m = n = 0$), have been termed zonal flows. Importantly, zonal flows emerge as a generic feature of different dynamical models independent of plasma conditions or the geometry, and are

a good example of self-organisation that can occur in complex systems with nonlinear interactions on many spatio-temporal scales [1-3].

The presence of zonal flows can modify drift wave turbulence transport via two mechanisms. First, simple energy balance suggests that the level of turbulence must decrease since the energy of the zonal flows is acquired directly from the turbulence through nonlinear interactions. Second, zonal flows naturally evolve into long-lived coherent structures that support stationary shear layers [4]. Spacially intermittent regions of high velocity shear exhibit decreased levels of transport since the shear distorts and destroys turbulent eddies. We recall here that, in a simple random walk approximation for the particle diffusion coefficient across the magnetic field, the eddy size represents the smallest step of the transport process. Thus zonal flows may be one of the important ingredients in the development of transport barriers which are observed during the transition from low to high confinement mode plasma states.

In this paper we study particle transport in magnetically confined fusion plasma using a modified Hasegawa-Wakatani (HW) model [5, 6] which produces drift wave turbulence that self-organises into zonal flows. We study the transport of passive test particles which are advected by the $E \times B$ velocity; see [6-17] for example. Our flexible model allows us to compare the case where zonal flows are absent to the case where zonal flows are self-generated and also to an intermediate state where the kinetic energy is shared equally between the zonal flows and drift wave turbulence.

The response of particles to turbulent fields can greatly differ depending on the Larmor radius. High frequency gyromotion effectively smooths out small fluctuations leading, intuitively, to a lower rate of transport. A reduction in radial transport with increasing Larmor radius was shown in [7-10] using the Hasegawa-Mima (HM) equation [18] as the turbulence model. More recently it was found that, in the limit of large Kubo number, $K > 1$, this reduction in transport is less dramatic and in some cases, the rate of transport may actually increase with the Larmor radius [11-14]. The Kubo number, $K = \langle v^2 \rangle^{1/2} \tau_c / \lambda$, is a measure of the average distance covered by a test particle $\langle v^2 \rangle^{1/2} \tau_c$, in one correlation time $\tau_c$, relative to the typical spatial scale of the turbulent fluctuations $\lambda$. In [14] it was reported that the zonal flow may have a strong influence on the rate of transport and on the Larmor radius dependence.

This paper is organised as follows. In the next section, the model of turbulence used in this study is described, namely the Hasegawa-Wakatani model. Section 3 illustrates the three different regimes of turbulence that are studied: drift wave turbulence with zonal flows damped, zonal flows allowed to dominate and an intermediate state. In section 4, the test particle studies are presented. Discussion and conclusions are given is sections 5 and 6.

## 2. Model equations

The HW model is a paradigmatic description of electrostatic turbulence in the edge region of a tokamak plasma, adopting the approximation of a non-uniform background

density and uniform equilibrium magnetic field. It generalises the simpler HM equation to include a nonadiabatic electron response due to parallel resistivity. This gives rise to an instability which is absent in the HM equation; in this respect the HW model provides a more complete description of drift wave turbulence. The equations for the electron density $n$ and the vorticity $\omega = \nabla^2\phi$, where $\phi$ is the electrostatic potential, are

$$\frac{\partial n}{\partial t} = -\kappa\frac{\partial \phi}{\partial y} + [n,\phi] + \alpha(\phi - n) + D\nabla^2 n \ , \tag{1}$$

$$\frac{\partial \omega}{\partial t} = [\omega,\phi] + \alpha(\phi - n) + \mu\nabla^2\omega \ , \tag{2}$$

where the Poisson bracket notation for nonlinear terms $[A,B] = \frac{\partial A}{\partial x}\frac{\partial B}{\partial y} - \frac{\partial A}{\partial y}\frac{\partial B}{\partial x}$ is used. Dimensionless variables are constructed using the mappings

$$\frac{e\phi}{T_e} \to \phi \ , \ \frac{n}{n_0} \to n \ , \ \omega_{ci}t \to t \ , \ \frac{x,y}{\rho_s} \to x,y \ , \tag{3}$$

where zero subscripts denote background quantities, $T_e$ is electron temperature, $\omega_{ci}$ is ion gyrofrequency and $\rho_s = \sqrt{m_i T_e}/eB$ is hybrid Larmor radius. Dissipation terms of the form $\nabla^2 f$ are added to the equations for numerical reasons and $D$ and $\mu$ are dissipation coefficients that mimic collisionality and viscosity. We assume that $\kappa = -\partial \ln n_0/\partial x$, controlling the background density profile $n_0(x)$, is a constant. The magnetic field is assumed to be uniform and pointing in the $z$ direction, $\mathbf{B} = B_0\hat{\mathbf{z}}$, and the $x$ and $y$ directions are identified respectively with the radial and poloidal directions of a tokamak. The model is cast into 2D by assuming a single parallel wavenumber $k$, so that the parameter

$$\alpha = \frac{T_e k^2}{n_0 e^2 \eta \omega_{ci}} \ , \tag{4}$$

controls the strength of the resistive coupling between $n$ and $\phi$ through the parallel current, where $\eta$ is electron resistivity. In the limit $\alpha \gg 1$ the coupling is adiabatic ($n = \phi$ in our normalised units) and the HW equations reduce to the HM equation.

In tokamaks, the zonal components ($k_y = 0$) of the potential and density do not contribute to the parallel current [19] and in the standard formulation of the equations (1 and 2), zonal flows are damped. Modified equations, which allow the self-generation of zonal flows, are obtained by removing the zonal components from the parallel coupling terms [20]:

$$\frac{\partial n}{\partial t} = -\kappa\frac{\partial \phi}{\partial y} + [n,\phi] + \alpha(\tilde{\phi} - \tilde{n}) + D\nabla^2 n \ , \tag{5}$$

$$\frac{\partial \omega}{\partial t} = [\omega,\phi] + \alpha(\tilde{\phi} - \tilde{n}) + \mu\nabla^2\omega \ , \tag{6}$$

where $\tilde{\phi} = \phi - \langle\phi\rangle$ and $\tilde{n} = n - \langle n\rangle$ are the non-zonal components and angular brackets denote the zonal components. In 2D the zonal component is simply the average over the poloidal $y$ direction,

$$\langle f\rangle = \frac{1}{L_y}\int f dy \ . \tag{7}$$

We refer to equations 1 and 2 as the Hasegawa-Wakatani (HW) equations and equations 5 and 6 as the modified Hasegawa-Wakatani (MHW) equations. The MHW equations were used to study the generation and stability of zonal flows in [20] and the interaction between drift wave turbulence and zonal flows in [21].

We solve equations 1 and 2, or 5 and 6, on a square of side $L = 40$ using $256 \times 256$ grid nodes with periodic boundary conditions. We use the third order Karniadakis time integration scheme [22] and the finite differences method for spatial discretisation with the Poisson bracket being computed through Arakawa's method [23]. This combination of numerical methods was introduced in [24] and tested in [25]. The parameters are set to $\kappa = 1$, $\alpha = 0.5$ and $D = \mu = 0.01$ for every case considered in this paper. The same set of parameters were used in a recent study [6], where the effect of non-uniform magnetic field strength on the turbulence and transport of passive test particles was studied.

## 3. Properties of the turbulence

### *3.1. Saturated turbulent state*

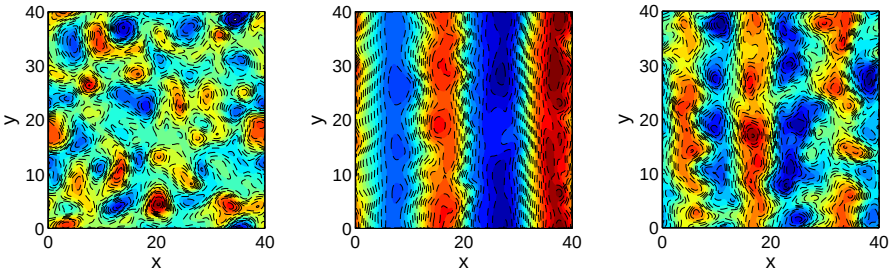


**Figure 1.** Snapshot of potential $\phi$ in the saturated quasi-stationary turbulent state for three related models: (left) HW defined by equations 1 and 2 where zonal flows are damped; (centre) MHW defined by equations 5 and 6 allowing the self-generation of zonal flows; (right) intermediate state of MHW where total kinetic energy of zonal flows is set equal to that of non-zonal drift wave turbulence at each time step.

Runs of the code are started with low-amplitude random noise. Linear drift waves are excited and grow exponentially until nonlinear effects become important. Eventually, a quasi-stationary saturated turbulent state is reached. In figure 1 we show typical snapshots of the potential $\phi$ in the quasi-stationary saturated turbulent state for the three cases considered. For the HW model, turbulent vortices dominate. For the MHW model, zonal flows dominate; while the zonal flows visible in figure 1 persist throughout the simulation time, inspection of the power spectrum reveals the presence of higher frequency broadband turbulence, because the drift wave turbulence has been suppressed but not eliminated. We note that the dominance of the zonal flows follows from the efficiency of the zonal flow generation in 2D turbulence [21]. An intermediate state is generated by artificially setting the kinetic energy of the zonal flows equal to the

kinetic energy of the non-zonal drift wave turbulence at each time step in the saturated turbulent state of the MHW model,

$$\langle E\rangle_K \equiv \frac{1}{2}\int\left(\frac{\partial\langle\phi\rangle}{\partial x}\right)^2 dV = \frac{1}{2}\int(\nabla\tilde{\phi})^2\, dV \equiv \tilde{E}_K\ . \tag{8}$$

We find that zonal flows and turbulent vortices then coexist in a quasi-stationary state; the zonal flows in figure 1 persist throughout the simulation time.

### *3.2. Weiss field*

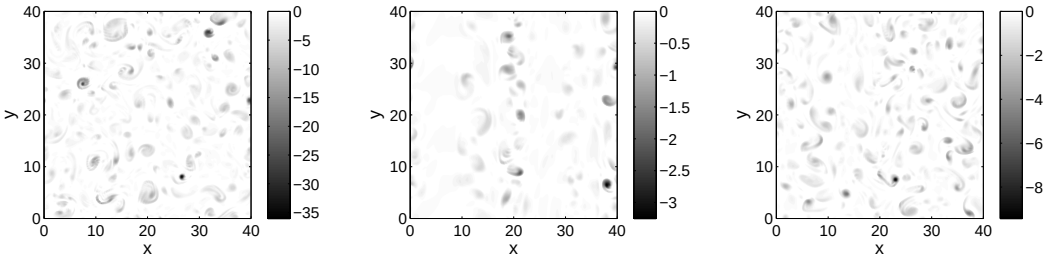


**Figure 2.** Weiss field, $Q$, calculated from data in figure 1: (left) HW; (centre) MHW; (right) intermediate state. Only negative values of $Q$ are shown.

Before the effects of finite Larmor radius on particle transport are considered in the next section, it is useful to provide a quantitative measure of the interaction between test particles and the coherent structures of the turbulent flow. For this purpose we employ the Weiss field, $Q$, [26] which is a local measure of stress $s$ compared to vorticity $\omega$. In the 2D velocity field provided by our model, $Q$ is defined as:

$$Q = \frac{1}{4}(s^2 - \omega^2)\ , \tag{9}$$

where the stress $s$ is given by

$$s^2 = \left(\frac{\partial v_x}{\partial x} - \frac{\partial v_y}{\partial y}\right)^2 + \left(\frac{\partial v_y}{\partial x} + \frac{\partial v_x}{\partial y}\right)^2\ , \tag{10}$$

and the vorticity is $\omega = \nabla^2\phi$. The $E\times B$ velocity field is given by equation 12. Thus $Q$ may be expressed as

$$Q = \left(\frac{\partial^2\phi}{\partial x\partial y}\right)^2 - \frac{\partial^2\phi}{\partial x^2}\frac{\partial^2\phi}{\partial y^2}\ , \tag{11}$$

which is equivalent to the second derivative test discriminant in calculus. Weiss showed [26] that if the strain rate varies slowly with respect to the vorticity gradient, the sign of $Q$ determines whether two initially close fluid elements will separate ($Q>0$) or not ($Q<0$), following the frozen streamlines. From the calculus point of view, $Q>0$ implies a local saddlepoint in $\phi$ while $Q<0$ implies a maximum or minimum. Evaluating $Q$ at the position of a test particle has been used to determine whether or not the particle is trapped in a nonlinear structure ($Q<0$) or not ($Q>0$) [10, 15]. In figure 2 we show the negative Weiss field, $Q<0$, calculated from the data in figure 1. Vortical

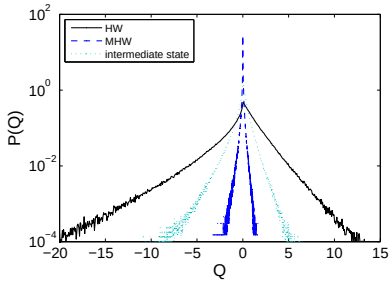


**Figure 3.** PDF of Weiss field, $P(Q)$, for the three turbulence regimes of figure 1.

structures are clearly distinguished by large negative values of $Q$. The probability density function (PDF) of $Q$, $P(Q)$, was shown in [27] to distinguish between different regimes of turbulence. Here, we calculate $P(Q)$ from multiple snapshots of the potential $\phi$ throughout the saturated turbulent state. Figure 3 shows $P(Q)$ on a semi-logarithmic scale for the three cases considered in figure 1, which $P(Q)$ clearly distinguishes. The negative tail, $Q < 0$, of the PDF falls off slowest for the HW case, fastest for the MHW case and is intermediate in the intermediate case. Therefore, we may expect trapping effects to be strongest in the HW case which has no zonal flows, weakest in the MHW case which has strong zonal flows, and intermediate in the intermediate case.

## 4. Test particle transport

We now turn to test particle transport and finite Larmor radius (FLR) effects. The form of the $E \times B$ velocity field,

$$\mathbf{v}_E = \left( -\frac{\partial \phi}{\partial y}, \frac{\partial \phi}{\partial x} \right) , \tag{12}$$

gives an indication of the FLR effects one would expect from our model. From equation 12 we conclude that contours of equipotential $\phi$ are stream lines of $\mathbf{v}_E$. Therefore, on time scales shorter than their life time, the turbulent structures – implying closed contours of $\phi$ – are impervious to test particles with zero Larmor radius. Conversely, test particles can be trapped by the structures, and the dynamics of the structures will affect the dispersion of the test particles. When the Larmor radius is finite, test particles are able to permeate turbulent structures, so that the effect of the structures on the transport is lessened.

For each value of Larmor radius $\rho$, a population of 10 000 test particles is initialised at random positions throughout the domain once the quasi-stationary turbulent state has been reached. The Larmor radius $\rho$ is measured in the dimensionless units of the model (equation 3), i.e. normalised to $\rho_s$. Provided that the frequency of the gyro-motion is much faster than the frequency of the turbulence, FLR effects can be included [7] simply by spreading the particle over a ring of (Larmor) radius $\rho$ centred on the particle's guiding centre. This is implemented numerically by averaging over $N_{\text{gyro}}$ ($= 16$ in this case) points. Each test particle has the equation of motion $\partial \mathbf{r}/\partial t = \hat{\mathbf{v}}_E$, where $\hat{\mathbf{v}}_E$ is the gyro-averaged $E \times B$ velocity given by equation 12. Bilinear interpolation

is used to calculate the potential $\phi$ at points away from grid nodes and the third order Karniadakis scheme [22] is used for time integration.

### *4.1. Test particle displacements*

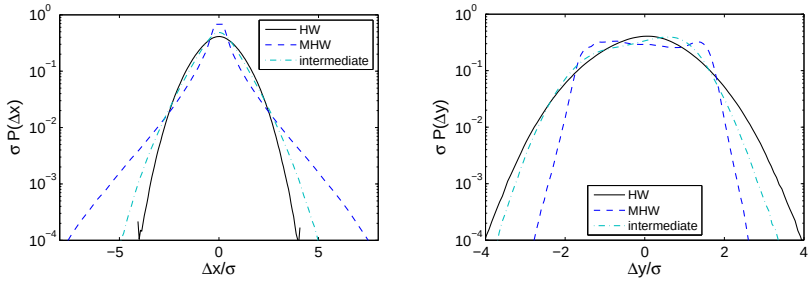


**Figure 4.** PDFs of jumps $\Delta x$ (left) and $\Delta y$ (right) made by particles for $\rho = 0$ in the HW, MHW and intermediate cases.

In figure 4 we plot the PDFs of the displacements $\Delta x$ and $\Delta y$ of test particles in the $x$ and $y$ directions for the three turbulence regimes represented by the three cases specified in figure 1. The PDFs $P(\Delta x)$ and $P(\Delta y)$ are plotted normalised to the standard deviation $\sigma$ and are calculated using the jumps made by the particles over one normalised time unit for the case where $\rho = 0$ for all test particles. We quantify departures of the distributions from Gaussian with skewness $S = \langle\Delta^3\rangle/\langle\Delta^2\rangle^{3/2}$, measuring asymmetry, and kurtosis $K = \langle\Delta^4\rangle/\langle\Delta^2\rangle^2$, measuring peakedness; a Gaussian PDF has $S = 0$ and $K = 3$. In the HW case we find $S = -0.01$ and $K = 3.00$ in the $x$ direction, and $S = -0.06$ and $K = 2.98$ in the $y$ direction; i.e. the PDFs are close to Gaussian. For the MHW case the PDFs are radically different and very far from Gaussian with $S = 0.00$ and $K = 8.06$ in the $x$ direction, and $S = 0.01$ and $K = 1.87$ in the $y$ direction. The PDFs for the intermediate state are indeed intermediate between the HW and MHW cases with $S = 0.00$ and $K = 4.01$ in the $x$ direction, and $S = -0.03$ and $K = 2.47$ in the $y$ direction. Similar PDFs are found when $\rho \neq 0$.

### *4.2. Test particle diffusion*

The Gaussian distribution of particle steps identified for the HW turbulence allows the assumption of diffusive transport in this regime. The significant departure of the PDFs from the normal distribution for the MHW and intermediate case raises intriguing questions about the nature of transport for these regimes. In this section, the nature of the test particle transport is established by examining running diffusion coefficients in the radial $x$ and poloidal $y$ directions. These are defined as follows:

$$D_x(t) = \frac{X(t)^2}{2t} \ , \ D_y(t) = \frac{Y(t)^2}{2t} \ . \tag{13}$$

Here $X(t)^2 = \langle[x(t) - \langle x(t)\rangle]^2\rangle$, $Y(t)^2 = \langle[y(t) - \langle y(t)\rangle]^2\rangle$ and $(x(t), y(t))$ is the position of the particle with respect to its initial position; angular brackets denote

an ensemble average over the 10 000 test particles. For a 'normal' diffusive process, with Gaussian steps that are uncorrelated, the running diffusion coefficient will reach a value independent of time since $X(t)^2 \sim t$. More generally the transport may be 'anomalous' and $X(t)^2 \sim t^\sigma$, where $0 < \sigma < 1$ implies subdiffusion and $1 < \sigma < 2$ implies superdiffusion. Our goal is to establish whether a diffusive transport model can be used for the test particles in the MHW and intermediate regimes, and also to determine if the nature of the transport is modified by FLR effects.

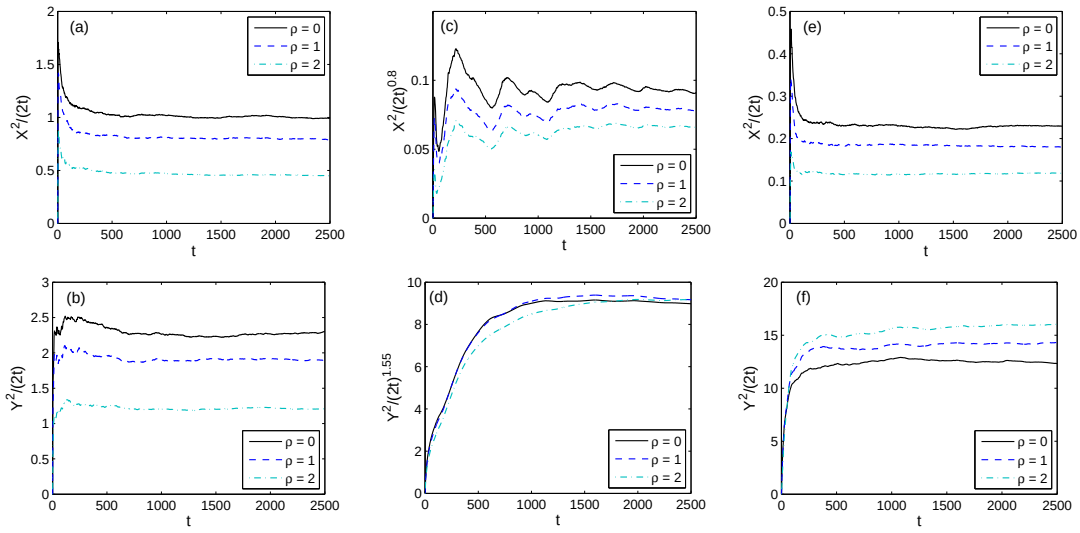


**Figure 5.** Test particle diffusion: (a) and (b) $X^2/2t$ and $Y^2/2t$ versus time for HW case showing normal diffusion; (c) and (d) $X^2/(2t)^{0.8}$ and $Y^2/(2t)^{1.55}$ versus time for MHW case demonstrating subdiffusion in $x$ and superdiffusion in $y$; (e) and (f) $X^2/2t$ and $Y^2/2t$ versus time for intermediate turbulence case showing normal diffusion.

In figure 5 (a) and (b) we plot the running diffusion coefficients $X^2/2t$ and $Y^2/2t$ versus time for the HW case for $\rho = [0, 1, 2]$. We find that these quantities converge on time independent values, indicating normal diffusive processes in both the $x$ and $y$ directions and for all values of $\rho$. We note that the rate of transport is larger in the poloidal $y$ direction than the radial $x$ direction by a factor of about two. These results agree with [15], where it was shown that passive test particle transport in the HW model is essentially a normal diffusive process arising from trapping and detrapping of the test particles by the turbulent vortices.

Figures 5 (c) and (d) show $X^2/(2t)^{0.8}$ and $Y^2/(2t)^{1.55}$ versus time for the MHW case. We find that these quantities become time independent, indicating that for all values of $\rho$, radial diffusion (across the zones) is subdiffusive with exponent $\sigma \approx 0.8$ while poloidal diffusion (along the zones) is superdiffusive with exponent $\sigma \approx 1.55$. Unlike the other two cases presented here, the measured exponents for the MHW case change slightly with different seeding of the turbulence code. We obtain exponents in the range $\sigma \approx 0.8 - 0.9$ in the radial direction and $\sigma \approx 1.5 - 1.8$ in the poloidal direction. We note that zonal flows drastically reduce radial transport and increase poloidal transport compared to the HW case. In the presence of zonal flows, poloidal

superdiffusion was found in [10] and [17] using the HM model and radial subdiffusion was found in gyrokinetic ITG turbulence in [28].

Figures 5 (e) and (f) show $X^2/2t$ and $Y^2/2t$ versus time for the intermediate turbulence case. In contrast to the MHW case, we find that the running diffusion coefficients converge on time independent values, indicating normal diffusive processes for all $\rho$. We note that the rate of transport is larger in the poloidal $y$ direction than the radial $x$ direction by about an order of magnitude. Compared to the HW case, the poloidal diffusion is about five times larger, while the radial diffusion is about five times smaller.

### *4.3. Larmor radius dependence*

In the previous section, we determined the nature of the test particle diffusion and established that this does not change with the Larmor radius, i.e. the exponent $\sigma$ is independent of $\rho$. In this section, we determine how the magnitude of the diffusion changes with the Larmor radius $\rho$. In figure 6 we plot the values of the diffusion coefficients $D_x$ and $D_y$ at the end of the simulation ($t = 2500$ normalised time units) as a function of $\rho$ for all the cases considered in order to show the trends. The results taken from the previous section, where all the test particles share the same Larmor radius $\rho$, are indicated by crosses. Circles indicate the results when the Larmor radii $\rho'$ are distributed around a most probable value $\rho$ according to a discrete approximation to the Boltzmann distribution,

$$f(\rho') = (4\pi^{-1/2}\rho^{-3})\rho'^2 \exp\left(-\rho'^2/\rho^2\right) . \tag{14}$$

We note that the results for the MHW case do not represent true diffusion coefficients since $D_x$ and $D_y$ change with time and the figures are plotted for comparison purposes.

Figures 6 (a) and (b) show the results for the HW case. For all cases, the diffusion coefficients decrease as $\rho$ increases. A transition between regions of faster and slower decline occurs around $\rho = 3$ which equates to the typical radius of the turbulent vortices seen in snapshots of the potential (figure 1).

Figures 6 (c) and (d) show the results for the MHW case. The Larmor radius dependence of the poloidal diffusion coefficient $D_y$ is radically different from the HW case. For small values of $\rho$, $D_y$ increases with $\rho$. For larger $\rho$, the rate at which $D_x$ and $D_y$ decline with increasing $\rho$ is smaller than in the HW case. For large values of $\rho$, the Larmor radius dependence of $D_y$ significantly differs between the case where all test particles share the same $\rho$ and the case where the Larmor radii follow a Boltzmann distribution. In the former case, $D_y$ falls off almost to zero at $\rho = 8$ which corresponds to the radial half-wavelength of the zonal flow, so that the effects of the zonal flow are maximally averaged out. Although the exponents $\sigma$ change when the seeding of the turbulence code is changed–as discussed in the previous section–the features of the Larmor radius dependence described here do not change.

Figures 6 (e) and (f) show the results for the intermediate turbulence case. We find that the Larmor radius dependence has similarities to the MHW case. The radial

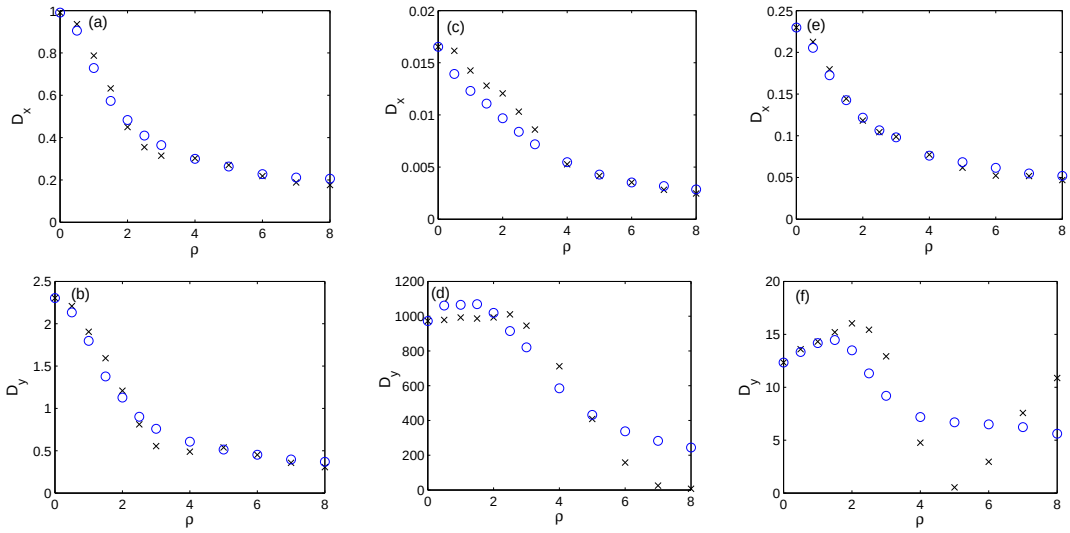


**Figure 6.** Value of diffusion coefficients $D_x$ and $D_y$ at the end of the simulation ($t = 2500$ normalised time units) as a function of $\rho$: (a) and (b) HW case; (c) and (d) MHW case; (e) and (f) intermediate turbulence case. Crosses indicate results when all the test particle share the same Larmor radius $\rho$; circles indicate results when the Larmor radii are distributed around a most probable value $\rho$.

diffusion coefficient $D_x$ decreases with $\rho$. For small $\rho$, the poloidal diffusion coefficient $D_y$ increases with $\rho$, and this effect is larger than in the MHW case. For larger $\rho$, when all the test particles share the same Larmor radius, $D_y$ decreases to a minimum around $\rho = 5$ and this corresponds to the radial half-wavelength of the zonal flow. The value of $D_y$ at this minimum is very close to the corresponding value for the HW case. When the test particles have a Boltzmann distribution of Larmor radii, there is no such minimum, and $D_y$ falls off slowly with large $\rho$.

## 5. Discussion

Several interesting effects for test particle transport in the presence of zonal flows have been identified. The introduction of strong zonal flows modifies the distribution of particle steps significantly. This is accompanied by a radical change in the nature of transport, which is no longer diffusive. While we are able to identify subdiffusive radial transport and superdiffusive poloidal transport, the convergence to these regimes is slow and the exact values of the scaling exponents $\sigma$ appear not to be universal since their values depend on the initial conditions.

In the intermediate regime the PDFs also depart from Gaussian, but the transport process can still be described as diffusion. While this behaviour is qualitatively similar to the HW case, the values of the diffusion coefficients are radically different with $D_x$ decreasing and $D_y$ increasing by an order of magnitude.

With zonal flows present, when all test particles share the same Larmor radius, $D_y$ falls off with $\rho$ to a minimum which corresponds to the half-wavelength of the zonal

flow. This minimum might be expected since test particles with $\rho$ equal to the half-wavelength of the zonal flow will sample one full period of the zonal potential, leading to a low rate of poloidal transport since the sum over one period should be close to zero. No such minimum occurs when the test particles have a Boltzmann distribution, because a significant fraction of the test particles then have Larmor radii not equal to the zonal flow half-wavelength.

Intuitively, increasing the Larmor radius $\rho$ should lead to a decrease in diffusion since increasingly large fluctuations are averaged out, as seen in HM simulations [10]. In the HW case defined by equations 1 and 2, we observe this decrease. However, when zonal flows and turbulent vortices coexist (as in the MHW and intermediate cases defined by equations 5 and 6) we find that the poloidal diffusion $D_y$ increases with $\rho$ for small $\rho$. This may be explained by the fact that increasing $\rho$ also decreases the amount of trapping due to turbulent vortices. When $\rho$ is small, test particles can be trapped in vortices and effectively shielded from the zonal flow. As $\rho$ is increased the amount of trapping is reduced, so that the test particles are more exposed to the zonal flow potential, leading to an increase in $D_y$. This effect is stronger in the intermediate case than in the MHW case, due to the presence of larger turbulent vortices, as evidenced in section 3.2. No increase in $D_x$ is observed, because zonal flows do not produce radial diffusion.

## 6. Conclusions

We have investigated the effect of finite Larmor radius on the transport of passive test particles moving in turbulent electrostatic fields modelled by different variants of the Hasegawa-Wakatani equations. A wide variety of transport phenomena were observed due to an interplay between trapping in small scale vortices and entrainment in larger scale zonal flows. This flexible model allows the comparison of the case where zonal flows are damped, the case where zonal flows are self-generated and an intermediate state where the kinetic energy is shared equally between the zonal flows and drift wave turbulence.

We have established that, with zonal flows damped, the test particle transport is classically diffusive, with Gaussian statistics, and the rate of transport decreases with increasing Larmor radius. Once the Larmor radius is larger than the typical radius of the turbulent vortices, the rate of transport remains roughly constant.

When self-generating, poloidally extended zonal flows are allowed, non-Gaussian PDFs of test particle displacements are produced, the rate of radial transport is reduced, the rate of poloidal transport is increased and the Larmor radius dependence is altered. The rate of poloidal transport increases with small values of the Larmor radius and this may be attributed to a reduction in trapping effects due to the turbulent vortices, which shield particles from the zonal flows. When zonal flows are allowed to dominate, poloidal transport becomes superdiffusive and radial transport becomes subdiffusive.

**Acknowledgments**

This work was supported in part by the UK Engineering and Physical Sciences Research Council and by Euratom. JMD acknowledges support from an EPSRC CASE studentship in association with UKAEA. The content of the publication is the sole responsibility of the authors and it does not necessarily represent the views of the Commission of the European Union or their services.

[1] Diamond P H, Itoh S-I, Itoh K and Hahm T S 2005 *Plasma Phys. Control. Fusion* **47** R35
[2] Fujisawa A *et al* 2006 *Plasma Phys. Control. Fusion* **48** S205
[3] Tsuchiya H, Itoh S-I, Fujisawa A, Kamataki K, Shinohara S, Yagi M, Kawai Y, Komori A and Itoh K 2008 *Plasma Phys. Control. Fusion* **50** 55005
[4] Smolyakov A I, Diamond P H and Malkov M 2000 *Phys. Rev. Lett.* **84** 491
[5] Hasegawa A and Wakatani M 1983 *Phys. Rev. Lett.* **50** 682
[6] Dewhurst J M, Hnat B and Dendy R O 2009 *Phys. Plasmas* **16** 072306
[7] Manfredi G and Dendy R O 1996 *Phys. Rev. Lett.* **76** 4360
[8] Manfredi G and Dendy R O 1997 *Phys. Plasmas* **4** 628
[9] Annibaldi S V, Manfredi G, Dendy R O and Drury L O'C 2000 *Plasma Phys. Control. Fusion* **42** L13
[10] Annibaldi S V, Manfredi G and Dendy R O 2002 *Phys. Plasmas* **9** 791
[11] Vlad M and Spineanu F 2005 *Plasma Phys. Control. Fusion* **47** 281
[12] Vlad M, Spineanu F, Itoh S-I, Yagi M and Itoh K 2005 *Plasma Phys. Control. Fusion* **47** 1015
[13] Hauff T and Jenko F 2006 *Phys. Plasmas* **13** 102309
[14] Hauff T and Jenko F 2007 *Phys. Plasmas* **14** 92301
[15] Naulin V, Nielsen A H and Juul Rasmussen J 1999 *Phys. Plasmas* **6** 4575
[16] Naulin V, Garcia O E, Priego M and Juul Rasmussen J 2006 *Phys. Scr.* **T122** 129
[17] Gustafson K, del-Castillo-Negrete D and Dorland W 2008 *Phys. Plasmas* **15** 102309
[18] Hasegawa A and Mima K 1978 *Phys. Fluids* **21** 87
[19] Dorland W and Hammett G W 1993 *Phys. Fluids B* **5** 812
[20] Numata R, Ball R and Dewar R L 2007 *Phys. Plasmas* **14** 102312
[21] Scott B D 2005 *New J. Phys.* **7** 92
[22] Karniadakis G E, Israeli M and Orzag S O 1991 *J. Comput. Phys.* **97** 414
[23] Arakawa A 1966 *J. Comput. Phys.* **1** 119
[24] Naulin V 2003 *Phys. Plasmas* **10** 4016
[25] Naulin V and Nielsen A 2003 *SIAM J. Sci. Comput.* **25** 104
[26] Weiss J 1991 *Physica D* **48** 273
[27] Bos W J T, Futatani S, Benkadda S, Farge M and Schneider K 2008 *Phys. Plasmas* **15** 72305
[28] Sanchez R, Newman D E, Leboeuf J -N, Carreras B A and Decyk V K and 2009 *Phys. Plasmas* **16** 055905